Research Square

Preprints are preliminary reports that have not undergone peer review.
They should not be considered conclusive, used to inform clinical practice,
or referenced by the media as validated information.

Paired genomic profiling reveals a continuum of genomic relatedness in synchronous endometrial and ovarian carcinomas

Floriana Camarda
Fondazione Policlinico Universitario Agostino Gemelli IRCCS
Andrea Gazzo
Fondazione Policlinico Universitario Agostino Gemelli IRCCS
Luca Mastrantoni
luca.mastrantoni01@unicatt.it

Università Cattolica del Sacro Cuore
Michele Kulesko
Fondazione Policlinico Universitario Agostino Gemelli IRCCS
Simona Duranti
Fondazione Policlinico Universitario Agostino Gemelli IRCCS
Iolanda Mozzetta
Fondazione Policlinico Universitario Agostino Gemelli IRCCS
Angela Santoro
Fondazione Policlinico Universitario Agostino Gemelli IRCCS
Antonio D'Amati
Fondazione Policlinico Universitario Agostino Gemelli IRCCS
Valentina Iacobelli
Fondazione Policlinico Universitario Agostino Gemelli IRCCS
Rita Trozzi
Fondazione Policlinico Universitario Agostino Gemelli IRCCS
Giulia Sabetta
Fondazione Policlinico Universitario Agostino Gemelli IRCCS
Ilenia Marino
Fondazione Policlinico Universitario Agostino Gemelli IRCCS
Maria De Bonis
Fondazione Policlinico Universitario Agostino Gemelli IRCCS
Gian Franco Zannoni
Fondazione Policlinico Universitario Agostino Gemelli IRCCS
Francesco Fanfani

Fondazione Policlinico Universitario Agostino Gemelli IRCCS

Anna Fagotti

Fondazione Policlinico Universitario Agostino Gemelli IRCCS

Angelo Minucci

Fondazione Policlinico Universitario Agostino Gemelli IRCCS

Tommaso Mazza

Fondazione Policlinico Universitario Agostino Gemelli IRCCS

Camilla Nero

Fondazione Policlinico Universitario Agostino Gemelli IRCCS

Article

Keywords:

Posted Date: November 20th, 2026

DOI: https://doi.org/10.21203/rs.3.rs-11606873/v1

License: This work is licensed under a Creative Commons Attribution 4.0 International License.
Read Full License

Additional Declarations: No competing interests reported.

Paired genomic profiling reveals a continuum of genomic relatedness in synchronous endometrial and ovarian carcinomas

Authors:

Camarda F[1,2]*, Gazzo A[3]*, Mastrantoni L[2,4], Kulesko M[3], Duranti S[5], Mozzetta I[6], Santoro A[7], D'Amati A[7], Iacobelli V[1,2], Trozzi R[1,2], Sabetta G[1], Marino I[5], De Bonis M[8], Zannoni GF[7], Fanfani F[1,2], Fagotti A[1,2], Minucci A[8], Mazza T[3]*, Nero C[1,2]*

Affiliations:

1 Unit of Oncological Gynecology, Women's Children's and Public Health Department, Fondazione Policlinico Universitario Agostino Gemelli, IRCCS, Rome, Italy

2 Università Cattolica del Sacro Cuore, Rome, Italy.

3 UOS Computational Biology and Bioinformatics, Fondazione Policlinico Universitario Agostino Gemelli IRCCS, Rome, Italy.

4 Comprehensive Cancer Center, UOC Medical Oncology, Fondazione Policlinico Universitario Agostino Gemelli IRCCS, Rome, Italy.

5 Scientific Directorate, Fondazione Policlinico Universitario Agostino Gemelli IRCCS, Rome, Italy.

6 Data Collection Research Core Facility Gemelli Science and Technology Park (G-STeP), Fondazione Policlinico Universitario Agostino Gemelli IRCCS, Rome, Italy.

7 Pathology Unit, Department of Laboratory and Hematology Sciences Fondazione Policlinico Universitario Agostino Gemelli IRCCS, Sacred Heart Catholic University Rome, Italy.

8 Departmental Unit of Molecular and Genomic Diagnostics, Fondazione Policlinico Universitario Agostino Gemelli IRCCS, Rome, Italy.

*These authors contributed equally

Correspondence to: Dr Luca Mastrantoni, Medical Oncology, Università Cattolica del Sacro Cuore, Rome, Italy.

Tel: 0039-0630154979; Fax: 0039-063052132

E-mail: luca.mastrantoni01@unicatt.it (L. Mastrantoni).

Abstract

Distinguishing independent synchronous primaries from metastatic dissemination in synchronous endometrial and ovarian carcinomas (SEOCs) is challenging since clinicopathologic features alone are insufficient to establish clonal relatedness without direct pairwise genomic comparison. We performed paired comprehensive genomic profiling of matched endometrial–ovarian tumors from 21 patients with presumptive SEOC, using the TSO500HT assay within a prospective institutional program (NCT06020625), characterizing shared and private mutations, directional imbalance, copy-number architecture, mutational signatures, and germline context. Eighteen of 21 pairs shared more variants than unrelated tumors, yet profiles spanned a continuum of relatedness, from highly shared configurations to pairs with no shared mutations and discordant copy-number patterns, rather than a binary of independent primaries or metastatic dissemination. Neither mutational process nor germline predisposition consistently determined tumor-pair configuration. These findings support reconceptualizing SEOCs as a clinicopathologic presentation encompassing heterogeneous biological states and establish that paired profiling provides an interpretive layer that individual tumor features cannot substitute.

Introduction

Synchronous endometrial and ovarian carcinomas (SEOCs), formally recognized within the 2023 FIGO framework for endometrial cancer staging[1], account for up to approximately 10% of ovarian and 3–5% of endometrial cancer diagnoses[2,3]. When carcinoma is identified at both sites at diagnosis, the central question is whether the lesions represent truly independent primary tumors or metastatic spread between the two sites, a distinction that affects stage assignment, prognostic interpretation, adjuvant treatment planning, and the consensus reached during multidisciplinary tumor board discussion.

This distinction has historically relied on clinicopathologic algorithms, most notably the criteria proposed by Scully and by Ulbright and Roth, which use morphologic features including histotype, tumor grade, depth of myometrial invasion, lymphovascular space invasion (LVSI), ovarian laterality, ovarian surface involvement, and the presence of endometriosis[4,5]. These criteria remain deeply embedded in routine diagnostic practice and currently represent the only validated tools for primary-site assignment, with low-grade, organ-confined endometrioid tumors involving the endometrium and a unilateral ovary regarded as the prototypical synchronous presentation [1].

Over the past decade, genomic studies have substantially reshaped this field. Whole-exome and targeted sequencing analyses have shown that many apparently synchronous endometrioid endometrial-ovarian carcinomas are clonally related, supporting a shared origin rather than truly independent tumorigenesis [6,7]. Critically, this discordance is most evident in cases that clinicopathologic criteria would classify as independent primaries: Anglesio et al. reported clonal relatedness in 10 of 11 such cases [8], and subsequent series have consistently confirmed extensive overlap in driver alterations between uterine and ovarian components, irrespective of conventional morphologic classification[9–11]. Some cohorts have interpreted the pattern of shared alterations as pointing toward a shared endometrial origin[12,13], although the inferential basis for these directional conclusions varies substantially across studies.

At the same time, the genomic landscape of SEOCs is not uniform. A minority of paired tumors are genomically independent, including cases reported in the setting of mismatch repair deficiency (MMRd) and Lynch syndrome[14], and a smaller subset shows partial overlap with marked site-specific divergence that fits neither category[15]. Collectively, these data suggest that the biology of SEOCs may not be adequately captured by a rigid binary distinction and support a more integrated framework in which molecular profiling is used not only to test relatedness but to characterize the degree and pattern of genomic sharing.

In this study, we performed a retrospective single-center analysis of clinically defined SEOCs integrating paired comprehensive genomic profiling (CGP) with histopathologic and germline data. The primary objective was to determine whether SEOCs represent a strictly dichotomous diagnostic category or are instead distributed along a continuum of genomic relatedness, combining mutation sharing, directional private-variant imbalance, copy-number comparison, mutational process analysis, and clinicopathologic context. Relatedness metrics were computed for all pairs, and representative pairs from each molecular subgroup were then examined in detail to illustrate the range of configurations observed.

Results

Analytical cohort composition and molecular subgroups

Between January 2022 and December 2024, within the monocentric comprehensive cancer genome profiling program FPG500, 1,458 ovarian and 1,112 endometrial carcinomas were profiled. After restricting to epithelial tumors analyzed with the TruSight Oncology 500 High-Throughput (TSO500HT) assay and requiring paired endometrial-ovarian sequencing, 21 patients (42 matched tumor samples) remained for analysis (Supplementary Figure 1). One case (ID20) was excluded after one tumor component failed genomic quality.

Molecular subgroups, integrating somatic alterations, immunohistochemistry, and germline data, were assigned at the patient level. Three patients comprised a study-defined proofreading-polymerase-mutant subgroup (hereafter POLmut): two harbored pathogenic *POLE* exonuclease-domain variants (ID6 and ID19), and one harbored a *POLD1* exonuclease-domain variant (ID2). Three were considered MMRd-Lynch, two MMRd-non-Lynch, and 13 Other cases (see Methods).

Clinicopathologic features

Clinicopathologic characteristics are summarized in Figure 1a and Supplementary Table 1.

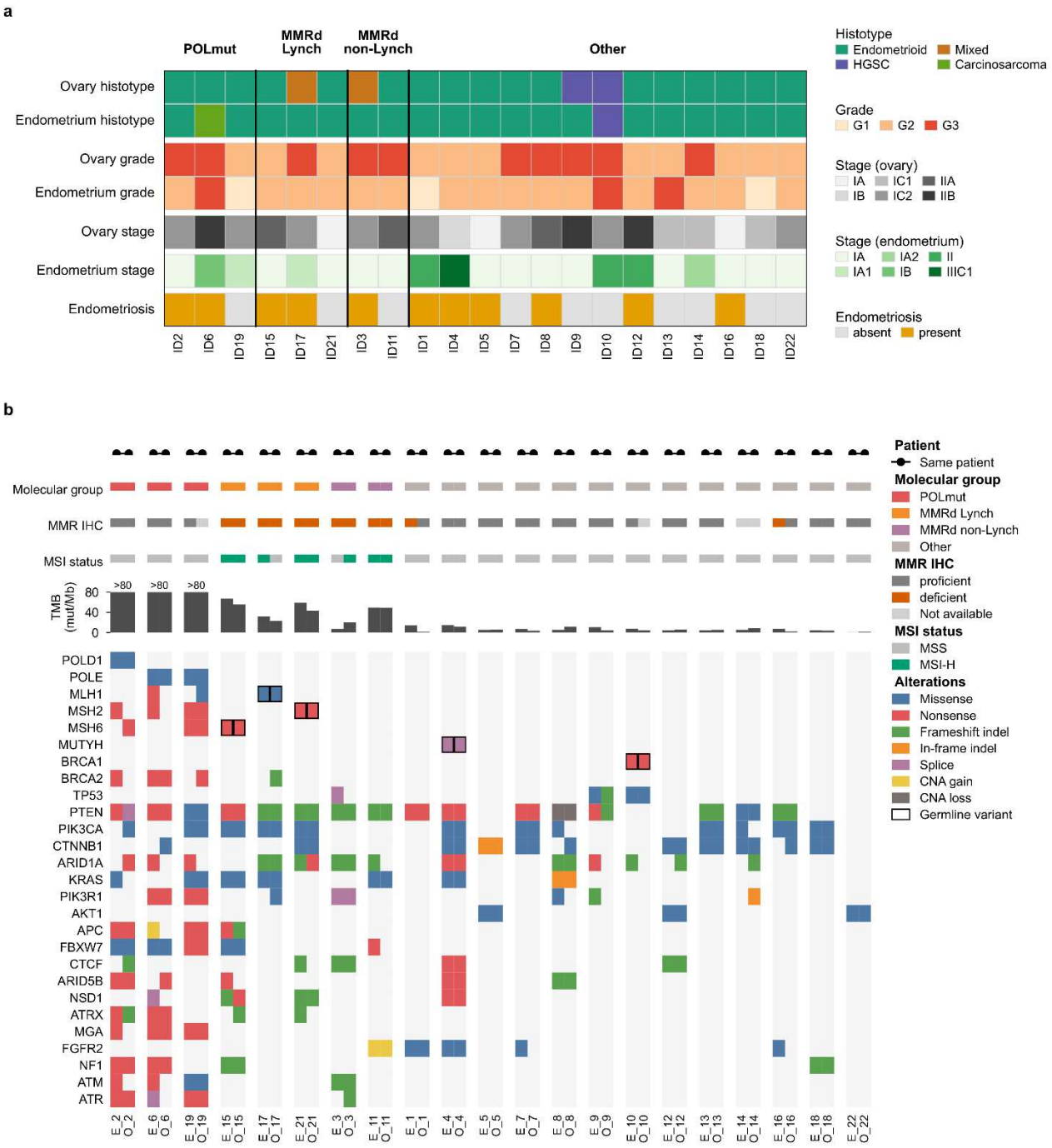


Figure 1 | Clinical and genomic landscape of synchronous endometrial–ovarian carcinomas.

a Clinicopathologic characteristics of the 21 patients, grouped by molecular subgroup (POLmut, MMRd Lynch, MMRd non-Lynch and Other). Each column represents one patient; histotype, grade and FIGO stage are shown separately for the ovarian and endometrial tumors, and endometriosis as present or absent. HGSC, high-grade serous carcinoma; Mixed, mixed clear cell–endometrioid carcinoma. **b** Integrated molecular profile of the 42 tumor samples. Each column represents one tumor (E, endometrium; O, ovary); tumors from the same patient are adjacent and joined by the indicator at the top. The upper tracks show molecular subgroup, mismatch repair (MMR) immunohistochemistry, microsatellite instability (MSI) status and tumor mutational burden (TMB, mutations/Mb; bars truncated at 80 and marked >80; exact values in Supplementary Table 1). The lower panel shows somatic alterations in selected cancer-associated genes, colored by functional class, together with copy-number gains and losses; germline variants present in the retained tumor variant set are outlined in black (the heterozygous CHEK2 variant of ID7 and MUTYH variant of ID9 are not part of this set and are not shown; see Supplementary Table 2).

Endometrioid histology predominated in both sites (19/21 endometrial; 17/21 ovarian), with concordant histotypes in 17 pairs. Four pairs (ID3, ID6, ID9, ID17) exhibited histologic discordance: mixed clear cell–endometrioid ovarian histology paired with endometrioid endometrial carcinoma (n = 2), endometrial carcinosarcoma paired with endometrioid ovarian carcinoma (n = 1), and ovarian high-grade serous carcinoma (HGSC) paired with endometrioid endometrial carcinoma (n = 1). Most endometrial tumors were low- or intermediate-grade (18/21), FIGO stage I at diagnosis (17/21), and showed superficial myometrial invasion (17/21); 15/21 met all three criteria. Ovarian tumors showed greater grade heterogeneity and were predominantly unilateral, although bilateral ovarian involvement occurred in five patients. Endometriosis was histologically documented in 11 patients. Hematoxylin and eosin-stained sections of specimens profiled in this study are reported in Supplementary Figure 2.

Integrated genomic landscape

Figure 1b presents the integrated molecular landscape of all 42 matched tumor samples, encompassing molecular subgroup, mismatch repair (MMR) immunohistochemistry, microsatellite instability (MSI) status, tumor mutational burden (TMB), recurrent somatic alterations, copy-number changes, and clinically relevant germline variants. TMB was highest in POLmut and MMRd cases, consistent with the ultramutated and hypermutated phenotypes associated with polymerase proofreading deficiency and mismatch repair loss, respectively. At the patient level, considering somatic alterations detected in at least one tumor component, *PTEN* was the most frequently altered gene (16/21, 76%), followed by *ARID1A* (13/21, 62%), *PIK3CA* (12/21, 57%), and *CTNNB1* (11/21, 52%). *KRAS* and *PIK3R1* alterations were each observed in 7 patients (33%), whereas *TP53* alterations were identified in 3 patients (14%).

Clinically or biologically relevant germline variants were identified in seven patients (Supplementary Table 2). The three MMRd-Lynch cases carried pathogenic *MSH6*, *MLH1*, or *MSH2* variants. ID4 had MUTYH-associated polyposis (homozygous germline *MUTYH*). ID10 harbored a germline *BRCA1* truncating variant with loss of heterozygosity in both tumor components, consistent with biallelic inactivation and homologous recombination deficiency (HRD). ID7 carried a heterozygous *CHEK2* variant without biallelic involvement. ID9 carried a heterozygous *MUTYH* variant without biallelic tumor involvement.

Continuum of paired-tumor relatedness

To quantify paired-tumor architecture, we classified retained somatic variants as endometrial-private, shared, or ovarian-private for each matched pair (Figure 2a; Supplementary Table 3).

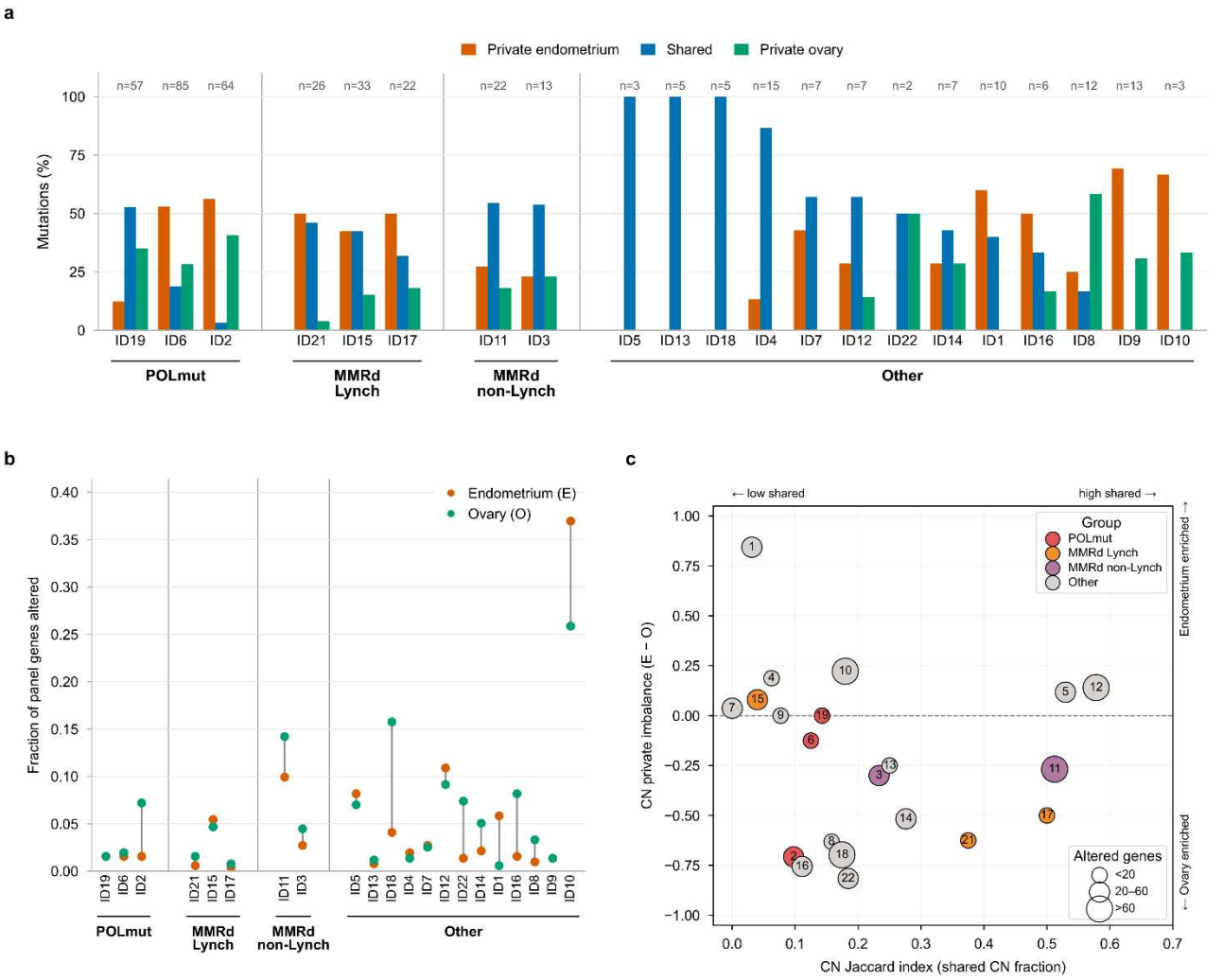


Figure 2 | Shared and private mutational architecture and copy-number divergence in synchronous endometrial–ovarian tumor pairs.

a Somatic mutations of each pair classified as private to the endometrium, shared between tumors, or private to the ovary, expressed as a percentage of all retained mutations in the pair; the total number of mutations is shown above each triplet. Pairs are grouped by molecular subgroup and ordered by decreasing shared fraction within each group. **b** Fraction of the 514 panel genes with a copy-number alteration in the endometrial (orange) and ovarian (green) tumor of each pair; lines connect tumors from the same patient. Patients are ordered as in a. **c** Copy-number concordance of each pair. The x axis shows the CN Jaccard index (genes with the same non-neutral copy-number state in both tumors divided by genes altered in at least one tumor); the y axis shows the CN private imbalance (endometrium-private minus ovary-private altered genes, divided by all altered genes; positive values indicate endometrium-enriched private alterations; distinct from the mutational directional imbalance). Point size indicates the number of altered genes, color the molecular subgroup, and the number the patient ID. In b and c, copy-number states are gene-level calls (median-centered log2 fold change ≥ 0.4, gain; ≤ −0.4, loss; see Methods).

Total retained variants ranged from 2 to 85 per patient, and shared fractions ranged from 0 to 1.0 (median 0.46, IQR 0.32–0.57; bootstrap 95% CI for the median 0.33 to 0.55). The highest variant counts occurred in POLmut cases: ID6 (85), ID2 (64), and ID19 (57). Despite comparable mutational burden, these three cases exhibited distinct architectures: ID2 (POLD1-mutant) shared 2/64 variants (3.1%, Wilson 95% CI 0.9–10.7%); ID6 (POLE-mutant) shared 16/85 (18.8%, Wilson 95% CI 11.9–28.4%), with a predominant endometrial-private compartment; and ID19 (POLE-mutant) shared 30/57 (52.6%, Wilson 95% CI 39.9–65.0%), with a higher shared fraction and ovarian-skewed private accumulation. This three-way difference in shared versus private variant counts was highly significant (chi-square test, $\chi^2 = 43.0$, df =

2, $p < 0.0001$), and each pairwise contrast remained significant (Fisher's exact test: ID2 vs ID6 $p = 0.0042$; ID2 vs ID19 $p < 0.0001$; ID6 vs ID19 $p < 0.0001$). Thus, proofreading-polymerase-associated ultramutation was associated with increased variant burden but did not correspond to a uniform paired-tumor architecture.

Low-sharing configurations were most evident in ID9 (0/13 shared variants) and ID2 (2/64 shared). ID10 also lacked shared variants, although with only three retained variants. Conversely, ID4 exhibited a strongly shared architecture (13/15 variants shared). ID5, ID13, and ID18 also showed complete mutational overlap, although each harbored only 3-5 total variants, cautioning against over-interpretation of apparent high genomic sharing in low-burden cases. Most cases (14/21) occupied intermediate positions, with shared fractions between 0.10 and 0.70. To estimate how much variant sharing can arise by chance between unrelated tumors, we created mismatched pairs by combining the endometrial tumor of each patient with the ovarian tumor of every other patient ($21 \times 20 = 420$ mismatched pairs; see Methods). Because a variant was counted as shared only when the identical nucleotide change was present in both tumors, mutations in the same gene but at different positions did not contribute to sharing. Unrelated tumors almost never shared variants: 370 of the 420 mismatched pairs (88%) shared none, the median shared fraction was 0.00, and 95% of mismatched pairs had a shared fraction of 0.04 or lower. Eighteen of the 21 true pairs had a shared fraction above this range, whereas ID2 (0.03), ID9 (0.00), and ID10 (0.00) fell within the range observed between unrelated tumors.

Integration of shared fraction with directional imbalance (see Methods), defined as $(E-O)/(E+O)$, with positive values indicating endometrium-skewed and negative values indicating ovary-skewed private-variant burden, showed distinct patterns across molecular subgroups (Supplementary Table 3). Directional imbalance was evaluable in 18 cases with at least one private variant. The three MMRd-Lynch cases showed consistent endometrial-skewed imbalance (range 0.47–0.86), despite intermediate shared fractions. This pattern was not mirrored by site-specific FIGO stage: the ovarian component was assigned a higher stage than the matched endometrial tumor in ID15 and ID17, whereas stages were matched in ID21 (Figure 1a). POLmut tumors were the most dispersed, spanning the full range of configurations: ID2 combined a very low shared fraction (0.03; 2/64) with near-neutral, mildly endometrium-skewed imbalance (+0.16); ID6 showed endometrium-skewed imbalance (+0.30) at a low-to-intermediate shared fraction (0.19; 16/85); and ID19 was the only POLmut case with ovary-skewed imbalance (−0.48), at a comparatively high shared fraction (0.53; 30/57). Ovary-skewed imbalance was also observed in the Other group, notably ID8 (shared fraction 0.17; imbalance −0.40).

Copy-number analysis added a further dimension to paired-tumor comparison (Figure 2b; Supplementary Table 3). Most pairs (17/21) showed low-to-moderate copy-number burden, with both components harboring <10% altered genes. Four cases (ID10, ID11, ID12, and ID18) had at least one component with 10% or more altered genes.

To distinguish copy-number burden from copy-number architecture, concordance was assessed among genes altered in at least one tumor component (Figure 2c; Supplementary Table 3). Genes were considered state-concordant when they carried the same non-neutral copy-number state in both tumors, whereas divergence reflected alterations restricted to one component or different non-neutral states across matched genes. Among the higher-burden pairs, ID11 and ID12 showed relatively concordant CNA profiles, with 42/82 (51.2%) and 37/64 (57.8%) altered genes, respectively, carrying the same non-neutral state in both tumors. In contrast, ID10 showed marked CNA divergence: 256 genes

were altered in at least one component (endometrial 37.0%; ovarian 25.9%), but only 46/256 (18.0%) were state-concordant, while the remainder were endometrial-private (n=123), ovarian-private (n=66), or altered in both tumors with different non-neutral states (n=21). ID18 showed the largest inter-site difference in CNA burden (ovarian 15.8%; endometrial 4.1%), with predominantly ovarian-private altered genes despite complete mutation overlap across only five retained variants. Across the cohort, the CN Jaccard index ranged from 0 to 0.58 (median 0.17, IQR 0.10–0.28; bootstrap 95% CI for the median 0.11 to 0.25), and the CN private imbalance (see Methods) ranged from −0.82 to +0.84 (median −0.25, IQR −0.62 to +0.08). Pair ranking was robust to the choice of threshold (Spearman ρ 0.82–0.84 at ±0.3 and ±0.5, and 0.80 with the caller's native gain/loss calls), and ID10 showed lower CN concordance than ID11 and ID12 at every threshold tested (Supplementary Table 4).

Across pairs, mutation sharing, private-variant imbalance, and copy-number architecture ranged from profiles with no shared alterations and divergent CNA states to highly shared profiles, with most cases showing intermediate or mixed patterns.

Ultra/Hypermutated subgroups: shared mutational processes with divergent architectures

In representative ultra/hypermutated pairs, shared dominant mutational processes coexisted with divergent paired-tumor architectures. Within each subgroup, pairs were selected to illustrate contrasting configurations; these case-level analyses complement the cohort-wide metrics shown in Figure 2 and Supplementary Tables 3 and 5, and all pairs are shown in Supplementary Figure 3.

Among POLmut tumors, concordant mutational signatures did not imply uniform paired tumor architecture. In ID2, both components were assigned by SigMA to its COSMIC v2-derived *POLE*-associated category (Supplementary Table 5); because that framework lacks a *POLD1*-specific category, the result was interpreted as a polymerase-proofreading-associated profile rather than as a *POLE*-specific attribution. Refitting to COSMIC v3.5 attributed 84% and 70% of substitutions in the endometrial and ovarian tumors, respectively, to SBS10d, the POLD1-associated proofreading signature, in keeping with the POLD1 exonuclease-domain variant (Supplementary Table 5). However, the paired mutation profile was largely private (36 endometrial-private, 26 ovarian-private, 2 shared; Figure 3a).

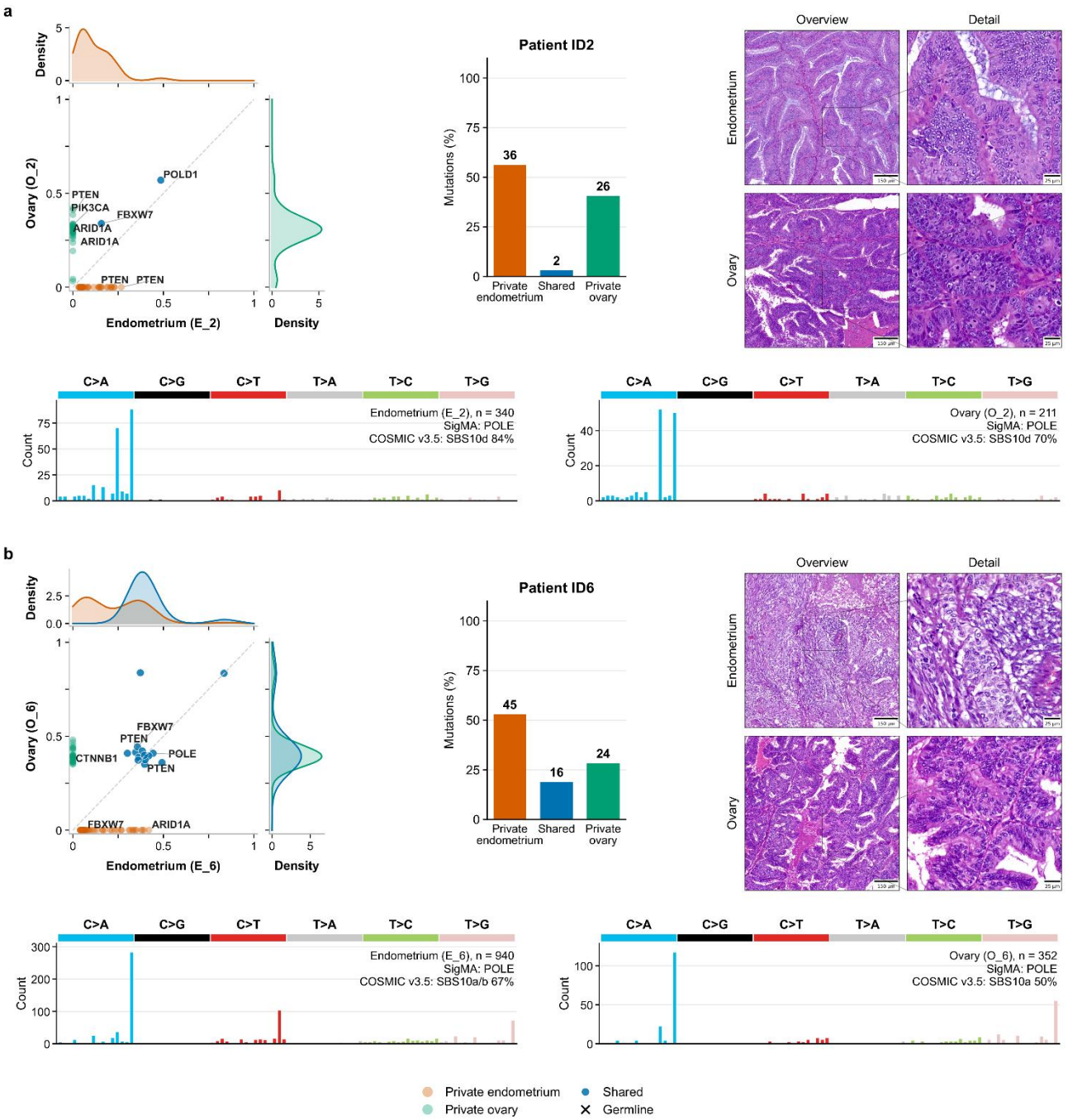


Figure 3 | Mutational architecture, signature profiles and histology of POLmut synchronous endometrial–ovarian tumor pairs.

a Patient ID2 (POLD1 exonuclease-domain variant). Top left, variant allele fractions (VAF) of retained variants in the endometrial (x axis) and ovarian (y axis) tumor, with marginal density plots; variants private to the endometrium, private to the ovary or shared are colored as indicated, confirmed germline variants are marked with a cross, and selected genes are labeled. Top center, shared and private mutations as a percentage of the pair total, with counts above the bars. Top right, representative hematoxylin and eosin-stained sections of the endometrial and ovarian tumors (overview, scale bar 150 µm; detail of the boxed area, scale bar 25 µm). Bottom, single-base-substitution profiles (SBS96) of the endometrial and ovarian tumors, generated from the broader single-nucleotide variant set used for mutational signature analysis (see Methods), annotated with the number of substitutions, the dominant SigMA signature and, for these POLmut tumors, the main polymerase-proofreading signature from COSMIC v3.5 refitting with its proportion of substitutions; within each substitution class, bars are ordered by 5' and then 3' flanking base (A, C, G, T). **b** Patient ID6 (POLE exonuclease-domain variant), displayed as in a.

Variant allele frequency (VAF) distributions mirrored this architecture, with most private variants confined to one compartment. The shared *POLD1* variant showed near-heterozygous VAFs in both

tumors, a pattern compatible with germline origin; however, germline testing was not performed because of patient refusal, and its constitutional or somatic origin could not be resolved. Histologically, the ovarian neoplasm was a grade 3 endometrioid carcinoma, with a solid-cystic pattern and areas of necrosis; while the endometrial sample was a grade 2 endometrioid carcinoma (Figure 3a). In contrast, ID6, also POLmut with dominant *POLE* signatures in both components (SBS10a/b in 67% and 50% of substitutions by COSMIC v3.5 refitting), retained a larger shared compartment (45 endometrial-private, 24 ovarian-private, 16 shared; Figure 3b). Polymerase-associated hypermutation was therefore linked to a high mutation burden but not to a fixed degree of variant sharing. Histologically, the endometrial tumor was a carcinosarcoma composed of a grade 3 endometrioid carcinomatous component (60%) and a high-grade sarcomatous component (40%). Genomic profiling was restricted to the endometrioid epithelial component, which was morphologically comparable to the paired grade 3 endometrioid ovarian carcinoma; the paired analysis therefore reflects epithelial-to-epithelial genomic divergence. In ID19, SigMA assigned the endometrial and ovarian tumors to the clock-like and MSI categories, respectively, whereas COSMIC v3.5 refitting attributed most substitutions to the POLE-associated SBS10a/b (60% and 59%), together with the MMR-associated SBS15 (33% and 23%; Supplementary Table 5).

Lynch-associated MMRd tumors exhibited a distinct pattern. In ID15 and ID21, both components displayed dominant MSI-associated signatures, sizeable shared compartments, and endometrial-enriched private burdens (ID15: 14 shared, 14 endometrial-private, 5 ovarian-private; ID21: 12 shared, 13 endometrial-private, 1 ovarian-private; Figure 4a,b).

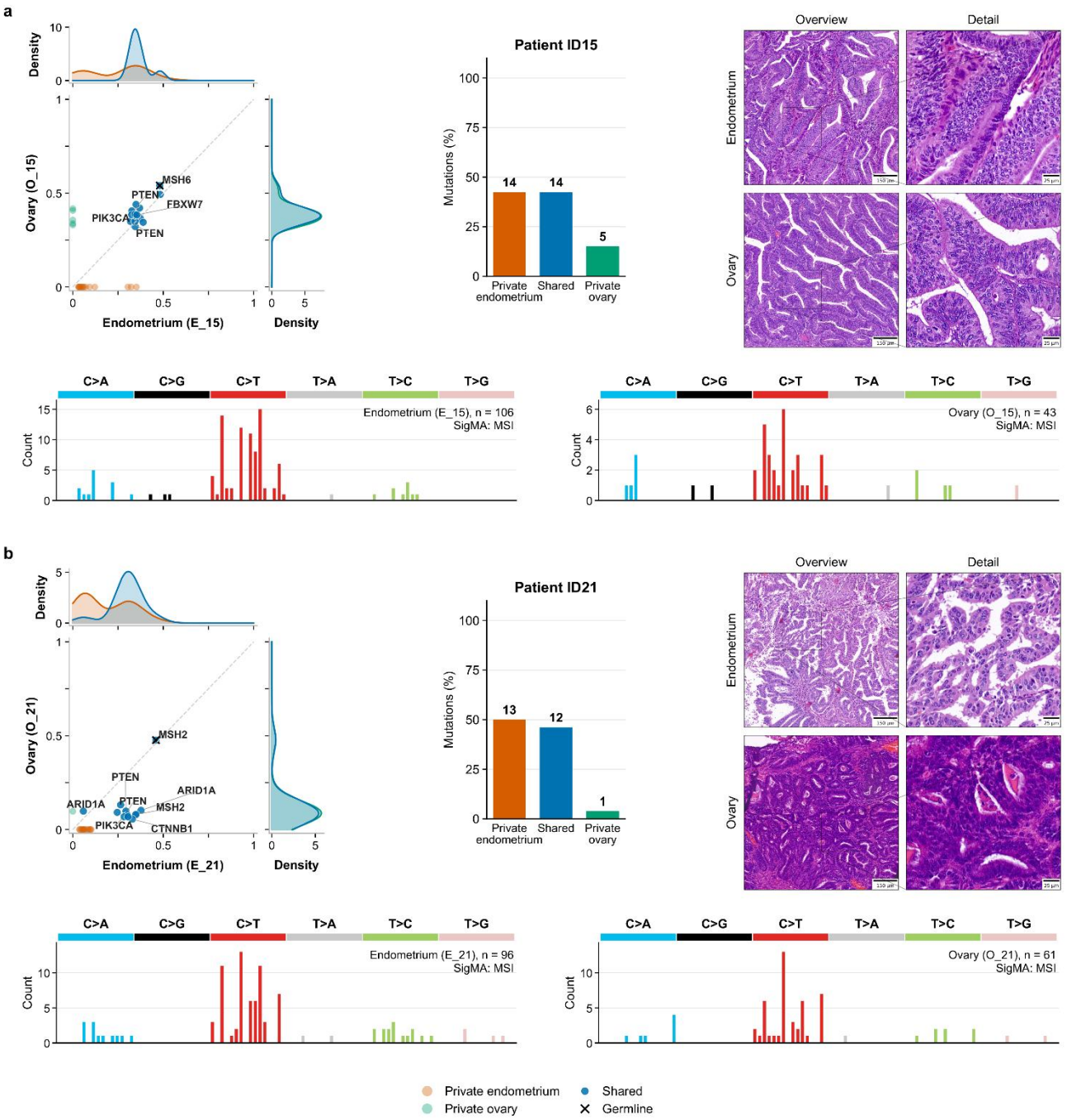


Figure 4 | Mutational architecture, signature profiles and histology of MMRd Lynch-associated synchronous endometrial–ovarian tumor pairs.

a Patient ID15 (germline MSH6 variant). **b** Patient ID21 (germline MSH2 variant). Both panels are displayed as in Fig. 3: VAF scatter plot with marginal densities, shared and private mutations, representative hematoxylin and eosin-stained sections (overview, scale bar 150 µm; detail, scale bar 25 µm), and SBS96 profiles of the endometrial and ovarian tumors with the dominant SigMA signature.

In both cases, VAF distributions supported the coexistence of shared alterations and site-specific private accumulation. Together with the cohort-level pattern across Lynch-associated cases, these pairs showed substantially shared genomic architecture with continued endometrial-enriched private variation. Both components of each patient were grade 2 endometrioid carcinoma. The third Lynch-

associated pair (ID17) showed the same endometrium-skewed private burden (directional imbalance 0.47; 7 of 22 variants shared; Supplementary Table 3).

Non-hypermutated subgroups: heterogeneous paired configurations

Non-hypermutated pairs further illustrated that germline or pathway context does not map directly onto a single paired-tumor architecture. ID9 carried a heterozygous *MUTYH* variant without biallelic tumor involvement and presented with histologically discordant tumors and a fully private variant profile (9 endometrial-private, 4 ovarian-private, 0 shared; Figure 5a).

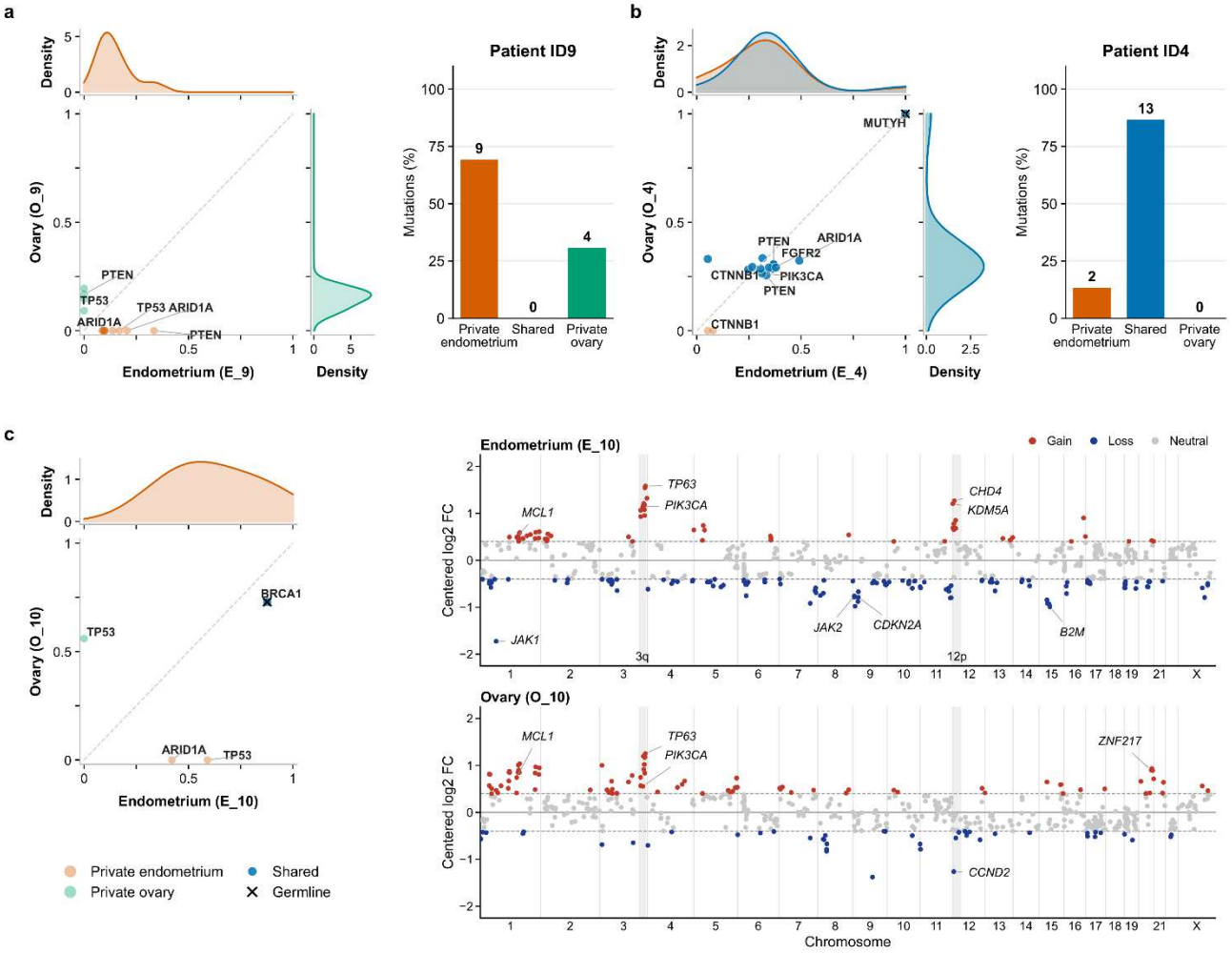


Figure 5 | Genomic evidence of distinct paired configurations in selected non-hypermutated synchronous endometrial–ovarian tumor pairs.

a Patient ID9 (heterozygous germline MUTYH variant; not part of the retained tumor variant set and therefore not shown). **b** Patient ID4 (homozygous germline MUTYH variant). In a and b, the left panel shows the VAF scatter plot and the right panel the shared and private mutations, as in Fig. 3. **c** Patient ID10 (germline BRCA1 truncating variant). Left, VAF scatter plot as in Fig. 3. Right, gene-level copy-number profiles of the endometrial (top) and ovarian (bottom) tumors: median-centered log2 fold change of each panel gene along the genome, with gains (≥ 0.4, red) and losses (≤ −0.4, blue); dashed lines mark the thresholds, shaded bands mark 3q26–q28 and 12p, and selected genes are labeled.

Accordingly, the ovarian tumor was an HGSC and the endometrial tumor a grade 2 endometrioid carcinoma. This pattern supports an independent-like genomic configuration, without implicating *MUTYH* as a shared tumor-driving mechanism.

Conversely, ID4, with a homozygous germline *MUTYH* variant, exhibited a strongly shared architecture (13 shared, 2 endometrial-private, 0 ovarian-private; Figure 5b). In the context of inherited predisposition, the shared germline variant is necessarily present at both sites; in ID4, however, the two tumors also shared a substantial fraction of somatic alterations, suggesting a genomic relatedness that extends beyond the common germline background.

ID10 exemplified a distinct CNA-dominant configuration. This patient carried a germline *BRCA1* truncating variant with loss of heterozygosity in both tumor components, consistent with biallelic *BRCA1* inactivation and HRD. Point mutations available for comparison were few: the shared *BRCA1* variant reflected the underlying germline predisposition, whereas the remaining point variants were site-specific (Figure 5c). The paired profiles were instead dominated by copy-number alterations (Figure 5c), which were extensive in both components (37.0% of the endometrial and 25.9% of the ovarian panel genes altered). Of the 514 panel genes, 256 were altered in at least one component; of these, only 46 (18.0%) shared the same non-neutral state in both tumors, while 210 (82.0%) were non-concordant—endometrial-private (n=123), ovarian-private (n=66), or discordant in state (n=21)—corresponding to a state-concordant CNA Jaccard index of 0.18. State-concordant alterations were concentrated on two chromosome arms: 22 of the 46 state-concordant genes were gains on 3q (n=12, including a contiguous block from TERC to TP63 at 3q26–q28, with PIK3CA and SOX2) and on 1q (n=10, including MCL1 and AKT3) (Figure 5c). Divergent alterations involved established cancer genes. The endometrial tumor alone carried losses of genes involved in interferon-γ signaling and tumor–immune interaction, including JAK1 (the deepest loss in either profile), B2M, JAK2, and the PD-L1 and PD-L2 genes CD274 and PDCD1LG2; the last three lie on 9p together with CDKN2A, which was also lost only in the endometrial tumor. In addition, genes on 12p were gained in the endometrial tumor (e.g., KDM5A and CHD4) and neutral or lost in the ovarian tumor (e.g., CCND2), and ZNF217 was gained only in the ovarian tumor. Interestingly, both the endometrial and the ovarian tumors were HGSC (Figure 1a). Thus, on a common germline BRCA1/HRD background, the two tumors shared gains of 3q and 1q, both recurrent in HGSC, while the remainder of their copy-number landscapes, including the immune-related losses of the endometrial tumor, diverged substantially, consistent with largely independent evolution of genomic instability in each component.

Discussion

Distinguishing truly independent primary tumors from metastatic disease in SEOCs remains challenging and has substantial clinical consequences including staging, adjuvant treatment decisions and genetic counseling. In current practice, classification still relies heavily on histopathologic criteria, and the classical presentation of low-grade endometrioid endometrial carcinoma paired with a unilateral low-grade endometrioid ovarian carcinoma is often regarded as a favorable synchronous phenotype [1,3]. However, accumulating genomic evidence indicates that this clinicopathologic presentation does not necessarily correspond to biologically independent primaries. By integrating mutational and copy-number profiles with clinicopathologic features and germline context, our study further challenges a rigid independent-versus-metastatic paradigm and instead supports a continuum of paired-tumor relatedness shaped by multiple layers of biology.

Across 21 clinically defined SEOC pairs, the proportion of shared somatic variants spanned the full range from zero to complete overlap, while directional private-variant imbalance and copy-number

differences introduced additional, partly orthogonal dimensions of heterogeneity. TMB-high tumors provided a clear illustration of the dissociation between mutational process and paired-tumor architecture. POLmut cases exhibited polymerase-associated signatures in both anatomic compartments (SBS10d in the POLD1-mutant case and SBS10a/b in the two POLE-mutant cases) yet showed markedly different degrees of variant sharing (for example, ID2 retained only two shared protein-altering variants out of 64, whereas ID6 shared 16 of 85): a pattern that extended to ID19 (30/57 shared) and was confirmed statistically across all three POLmut cases ($\chi^2 = 43.0$, $p < 0.0001$). In contrast, MMRd-Lynch cases consistently showed endometrial-skewed private burdens within sizeable shared compartments, linking their mutational process to a more reproducible, although still non-identical, paired architecture. These findings emphasize that mutational signatures capture operative processes, whereas shared/private architecture reflects compartment-specific divergence; one does not determine the other.

Germline predisposition further shaped paired-tumor configurations without imposing a single genomic pattern. ID4, with homozygous germline *MUTYH* alteration, showed extensive sharing of retained somatic variants and a highly shared genomic configuration despite its inherited background. By contrast, ID9 carried a heterozygous *MUTYH* variant and exhibited a fully private mutational profile consistent with a predominantly independent-like configuration. The *BRCA1*/HRD-associated case (ID10) illustrated a different dimension of complexity: biallelic *BRCA1* inactivation coincided with extensive CNA in both compartments, yet the paired profiles showed limited state-concordant CNA beyond shared 3q and 1q gains despite the shared HRD context, with losses of immune-related genes (JAK1, JAK2 and B2M) confined to the endometrial tumor. These observations caution against interpreting shared predisposition, hypermutation, or high CNA burden as sufficient evidence of relatedness in the absence of direct pairwise genomic comparison. They also argue for interpreting any individual shared fraction against the level of sharing expected by chance, since a panel restricted to recurrently mutated cancer genes will produce a non-zero baseline of sharing even between unrelated tumors of the same histotype; in our cohort, 50 of 420 mismatched pairs shared at least one variant, almost exclusively recurrent hotspots (e.g., PIK3CA R88Q, PTEN T319*, AKT1 E17K).

Taken together, our findings support a model in which clinically defined SEOC is not a single biological entity but a presentation encompassing independent-like, clonal-like, and intermediate genomic states. This continuum framework helps reconcile apparently discordant observations in the literature: some pairs harbor alterations shared across both tumors and show patterns compatible with genomic relatedness despite anatomic separation; others appear to arise independently within common environmental or inherited-risk contexts; and still others occupy intermediate positions, sharing a subset of somatic alterations while also showing substantial site-specific divergence. In this light, a binary classification may obscure biologically meaningful variation rather than resolve it.

This perspective has practical implications. In cases with discordant histology, high grade, hypermutation, or suspected hereditary predisposition, formal paired genomic analysis can refine interpretation beyond what morphology alone provides. Its value is not to relabel cases as independent or metastatic, but to characterize the degree and pattern of relatedness in a more biologically faithful way.

All analyses were based on routine clinical tumor-only panel sequencing, and the main constraints of the study follow from this design and from cohort size. This was a retrospective, single-center study of 21 patients, and outcome data (recurrence and survival) are not yet mature; prognostic associations

were therefore not assessed. Germline interpretation relied on separate germline testing, and residual germline variants escaping tumor-only filtering would appear as shared variants; this mainly affects pairs with few retained variants, whose shared fractions were interpreted accordingly. Mutational signatures were assigned as dominant processes with SigMA, which was developed for sparse panel data and has shown good performance in independent MSK-IMPACT validation studies [16,17]; calls were interpreted together with molecular subgroup, POLE/POLD1 status, and MSI/MMR phenotype, and in the POLmut pairs COSMIC v3.5 refitting resolved the polymerase-specific process. Copy-number states were derived from median-centered log2 fold changes without purity or ploidy adjustment, avoiding the propagation of model-dependent purity estimates from tumor-only panel data; because lower tumor content in one component would tend to reduce, rather than inflate, apparent concordance, copy-number concordance estimates are conservative, and pair rankings were stable across thresholds (Supplementary Table 4). Copy-number calls were made at the gene level: burden reflects the fraction of panel genes altered rather than the fraction of the genome, and shared breakpoints, the most specific copy-number evidence of common clonal origin, could not be resolved, so that recurrent events such as 3q and 1q gains may be shared through convergence as well as common descent. Cancer-cell-fraction inference and clonal/subclonal decomposition were not performed, as these estimates are unreliable from tumor-only targeted panels. Larger prospective studies integrating matched-normal sequencing, broader genomic coverage, cancer-cell-fraction modeling, and longitudinal follow-up will be required to validate the continuum framework and to determine how pairwise genomic architecture should inform staging, risk stratification, and treatment selection. Given the relative rarity of this presentation, adequately powered investigations will likely require collaborative integration of datasets across institutions.

Morphology remains indispensable, but it is not always sufficient: integrating shared and private mutations, directional imbalance, copy-number architecture, mutational signatures, germline context, and clinicopathology provides an additional interpretive layer that can reveal configurations otherwise missed by any single feature. More broadly, this integrated approach shifts the field away from a rigid independent-versus-metastatic dichotomy toward a biologically informed continuum model that better reflects tumor complexity and provides a foundation for future classification systems and clinical studies. Morphology remains indispensable, but it is not always sufficient: integrating shared and private mutations, directional imbalance, copy

Methods

Case selection

In January 2022, our institution launched a prospectively designed, real-world comprehensive cancer genomic profiling program (FPG500; NCT06020625). The program covers 11 tumor types, including endometrial cancer (EC) and ovarian cancer (OC), and enrolls unselected adult patients (18 years or older at the time of diagnosis). For the present study, we retrospectively interrogated the FPG500 registry to identify all patients evaluated between January 2022 and December 2024 who met the clinicopathologic definition of SEOC. Cases were eligible if both the endometrial and ovarian tumors were epithelial neoplasms and had been analyzed using the same high-throughput targeted sequencing platform (TruSight Oncology 500 High-Throughput [TSO500HT]). Cases were excluded if either tumor component lacked sequencing data, showed non-epithelial histology, or failed bioinformatic quality-

control filters. Consecutive case capture was used to limit selection bias and preserve the real-world heterogeneity of SEOCs encountered in clinical practice.

All patients provided written informed consent in accordance with the Declaration of Helsinki. The study protocol was reviewed and approved by the institutional review board (Protocol U 00194/23; approval ID 3837).

Molecular subgroup assignment

Tumor pairs were categorized at the patient level into biologically defined molecular subgroups. Pairs harboring pathogenic exonuclease-domain variants in *POLE* or *POLD1* were designated polymerase-mutant (POLmut), consistent with polymerase-associated ultramutated phenotypes[18]. Cases were classified as MMR-deficient at the patient level only when loss of MMR protein expression was concordant across the endometrial and ovarian components. Such pairs were assigned to the MMRd-Lynch subgroup when a pathogenic germline variant in an MMR gene (*MLH1*, *MSH2, MSH6*, or *PMS2*) was identified, and to the MMRd-non-Lynch subgroup when no germline MMR alteration was detected. Pairs with MMR deficiency restricted to one anatomic component or with indeterminate MMR immunohistochemistry were not assigned to the concordant MMRd groups and were retained in the Other group; individual results are reported in Supplementary Table 1.

All remaining pairs, without a pathogenic POLE/POLD1 exonuclease-domain variant and without concordant MMR deficiency (Lynch or non-Lynch), were grouped as 'Other'. This group is heterogeneous by construction; given the small numbers, no further subgroups (for example, by HRD or TP53 status) were defined. This subgrouping framework was used for subsequent clinicopathologic correlation and paired genomic analysis.

Histopathological assessment

Histopathologic data were abstracted from surgical pathology reports generated by a dedicated gynecologic pathology team operating within a standardized diagnostic framework. All available H&E-stained slides were centrally reviewed by three gynecologic pathologists (G.F.Z., A.S., and A.D.). Histotype and grade were reassessed according to the current WHO classification, with specific verification of the tumor component selected for genomic profiling. All patients underwent comprehensive surgical staging. Endometrial tumors were staged according to the FIGO classification in use at the time of diagnosis (FIGO 2009 or FIGO 2023); for patients staged before or concurrently with the release of the FIGO 2023 classification, the corresponding FIGO 2023 stage is additionally reported in Supplementary Table 1. Ovarian tumors were staged according to FIGO 2018. Unless otherwise specified, stage at diagnosis is reported throughout. For endometrial lesions, LVSI was classified as absent, focal, or substantial according to contemporary guidelines[1,19]. Immunohistochemical (IHC) evaluation of p53 and MMR proteins (MLH1, MSH2, MSH6, PMS2) was performed when clinically indicated. When next-generation sequencing identified *TP53* or MMR alterations discordant with IHC findings, clinical classification followed histopathologic interpretation, whereas discrepant molecular findings were retained for research analyses[20].

Clinicopathologic interpretation at diagnosis relied on established morphologic criteria traditionally used to distinguish synchronous primary tumors from metastatic disease[5,21]. Parameters considered included histotype concordance or discordance, tumor grade, depth of myometrial invasion, LVSI, ovarian laterality, and the presence of concurrent endometriosis. Although ESGO and FIGO staging frameworks provide structured approaches to the assessment of concomitant uterine and ovarian

involvement, expert review by dedicated gynecologic pathologists remained central to classification. In routine practice, all cases were prospectively designated as SEOCs following integrated morphologic assessment by three experienced gynecologic pathologists (G.F.Z., A.S., A.D.). These morphology-based classifications were retained as the reference diagnostic category for the present genomic study, enabling correlation between historical clinicopathologic interpretation and molecular findings.

Data collection

Demographic, clinical, and pathologic variables were prospectively captured in a customized electronic case report form (eCRF) using REDCap, a secure web-based platform compliant with the European Union General Data Protection Regulation (GDPR 2016/679). Clinical data were abstracted from the electronic medical record by one investigator (I.M.) and independently cross-checked by a second investigator (F.C.) to ensure completeness and accuracy. Discrepancies were resolved by consensus.

Genomic profiling and bioinformatic annotation

Targeted comprehensive genomic profiling was performed on formalin-fixed, paraffin-embedded tissue using the Illumina TruSight Oncology 500 High-Throughput (TSO500HT) assay. This hybrid-capture panel interrogates single-nucleotide variants, small insertions/deletions, copy-number alterations, tumor mutational burden, and microsatellite instability across 523 cancer-associated genes. Tumor samples were required to have adequate cellularity for variant detection, generally at least 20% of tumor content based on histopathologic assessment. Library preparation, sequencing, and primary data processing were performed according to the manufacturer's instructions. Raw sequencing reads were processed using the Illumina DRAGEN Solid pipeline (v2.5) with alignment to the GRCh37 (hg19) reference genome and subsequently annotated within the Clinical Genomics Workspace (Velsera).

Following primary variant calling, sequencing outputs were processed through Varan, an in-house bioinformatic workflow that harmonizes variant calls across samples and generates standardized mutation annotation format files [22]. Functional annotations were derived using the OncoKB knowledge base, and copy-number profiles were generated from aligned read counts.

For paired endometrial-ovarian comparisons, we used the variant set that underlies institutional clinical reporting, generated by Varan filtering and finalized at clinical molecular review. This curated set is restricted to coding and splice-region variants in OncoKB-annotated cancer genes and prioritizes alterations predicted to be functionally relevant [23].

A broader single-nucleotide variant (SNV) set was used for mutational signature refitting to maximize sensitivity for mutational process detection. Signature analysis included synonymous and non-coding SNVs retained after tumor-only quality filtering and germline-proxy filtering; indels were excluded. The parameter MAX_POP_AF was defined as the highest population allele frequency reported across 1000 Genomes and gnomAD, including subpopulation fields. Variants failing quality thresholds (non-PASS status, tumor depth below 50, alternate read count below 5, or variant allele fraction below 0.02) were excluded. Putative germline variants were filtered out when MAX_POP_AF was 0.01 or higher or, in tumor-only samples, when allele fractions were compatible with heterozygous (0.35–0.65) or homozygous (≥0.90) constitutional states in combination with MAX_POP_AF of 0.001 or higher or with an existing-variant annotation in public databases. Mutational signatures were inferred using Signature Multivariate Analysis (SigMA; v1.6, commit 92cf09c), a likelihood-based algorithm optimized for targeted sequencing panels [16]. The suitability of SigMA for panel-level dominant-process assignment has been further evaluated using MSK-IMPACT, a clinical panel of comparable genomic scale, by

benchmarking panel-derived calls against whole-exome or whole-genome reference data[17,24]. SigMA was applied to the broader SNV set to assign dominant mutational processes for each tumor. Endometrial and ovarian tumors were analyzed with the SigMA uterus and ovary tumor-type models, respectively, using the MSK-IMPACT 410-gene platform setting; per-tumor calls and likelihood scores are reported in Supplementary Table 5. Unless otherwise stated, paired analyses were based on the curated variant set, whereas mutational signature analysis used the broader SNV set to maximize the number of informative trinucleotide contexts. SigMA was applied with its original COSMIC v2-based reference, on which its panel-specific classifiers were developed and validated [16]. In this framework, polymerase-proofreading mutagenesis is represented by a single signature (Signature 10), whereas COSMIC v3.x separates POLE-associated (SBS10a/b) from POLD1-associated (SBS10c/d) processes, as well as combined polymerase-proofreading and MMR deficiency (SBS14, SBS20). The SigMA "POLE" category was therefore interpreted as polymerase-proofreading-associated rather than as a gene-specific attribution. To resolve the gene-specific polymerase process in the three POLmut pairs, whose ultramutated profiles provide several hundred SNVs per tumor, the same SBS96 profiles (generated with SigProfilerMatrixGenerator v1.3.6) were additionally refitted to COSMIC v3.5 reference signatures with SigProfilerAssignment (v1.1.3, GRCh37); per-tumor results are reported in Supplementary Table 5.

To account for variation in tumor cell content, tumor purity, ploidy, and loss of heterozygosity (LOH) were jointly inferred using PureCN (v2.12.0, R 4.4.3) [25]. For each sample, candidate solutions were independently reviewed using copy-number fits and somatic variant allele-frequency distributions, and the solution considered most biologically plausible was selected.

Each tumor report was reviewed by a geneticist to identify variants suspected to be of germline origin. Cases were referred for germline evaluation according to ESMO recommendations[26] or based on clinical assessment. Germline confirmation was performed on peripheral blood using Sanger sequencing for single-variant confirmation or, when clinically indicated, using a dedicated germline next-generation sequencing (NGS) panel.

Computational and statistical analyses

Downstream analyses were performed on curated variant, copy-number, clinicopathologic, and molecular annotation tables generated through the institutional bioinformatic pipeline. For each matched endometrial-ovarian pair, retained variants were compared using chromosome, genomic position, reference allele, and alternate allele to define unique variant identifiers. Variants meeting these criteria were classified as shared when the identical nucleotide change (chromosome, genomic position, reference allele, and alternate allele) was present in both tumors. Variants detected in only one component were classified as private to that anatomic site.

For each pair, we enumerated the number of shared variants (S), endometrial-private variants (E), and ovarian-private variants (O). Mutational similarity between paired tumors was summarized using the shared fraction, defined as:

Because the shared fraction is a proportion estimated from a variable number of retained variants per pair (range 2–85), a Wilson score 95% confidence interval was calculated for each pair's shared fraction to make this denominator-dependent uncertainty explicit; pairs with few retained variants necessarily have wide intervals. Shared versus private variant counts were compared between cases of similar

mutational burden using Fisher's exact test for pairwise contrasts and the chi-square test of independence for the omnibus comparison across more than two cases.

Background of chance sharing. To estimate the level of sharing expected between tumors that are not clonally related, we generated mismatched pairs by combining the endometrial tumor of each patient with the ovarian tumor of every other patient (21 × 20 = 420 mismatched pairs). Because the two tumors of a mismatched pair come from different patients, any variant they share reflects recurrence of the same mutation in the population rather than common clonal origin. For each mismatched pair, the shared fraction was calculated with the same variant set and matching criteria used for the true pairs (identical chromosome, position, reference allele, and alternate allele). The 95th percentile of the resulting distribution (0.04) was taken as the upper limit of chance sharing, and each true pair was described as above or within this range.

Private mutational asymmetry was quantified using the directional imbalance, defined as:

$$directional\ imbalance\ =\ \frac{(E-O)}{(E+O)}$$

Positive values indicate a relative excess of endometrial-private alterations, whereas negative values indicate ovarian-enriched private variation. Directional imbalance was considered not evaluable when no private variants were present. This measure was used to quantify site-specific asymmetry in private-variant burden and was not interpreted as evidence of metastatic directionality.

Copy-number profiles were compared at the gene level. Copy-number estimates were available as one fold-change value per panel gene (514 of the 523 assay genes, identical across samples); values were log2-transformed and median-centered within each sample. Genes with a centred log2 ratio ≥ 0.4 were classified as gains, those ≤ −0.4 as losses, and the remainder as neutral; the same thresholds were applied to both tumor components, and no purity or ploidy adjustment was applied. Endometrial and ovarian profiles were matched gene by gene, so that all 514 genes were compared in every pair. For each tumor component, the copy-number burden was calculated as the proportion of non-neutral genes among all evaluated genes. In paired analyses, altered genes were defined as the union of genes altered in at least one tumor component. These altered genes were classified as state-concordant when the same non-neutral copy-number state was present in both components, endometrial-private when altered only in the endometrial tumor, ovarian-private when altered only in the ovarian tumor, or discordant when altered in both tumors but with different copy-number states. Copy number alteration (CNA) concordance was summarized using a state-concordant Jaccard index, ranging from 0 (no state-concordant altered genes) to 1 (complete state concordance across all genes altered in at least one component), and calculated as the number of state-concordant altered genes divided by the total number of genes altered in at least one component. The CN private imbalance was defined as the number of endometrial-private minus ovarian-private altered genes divided by the number of genes altered in at least one component; positive values indicate an excess of endometrium-private alterations. This copy-number measure is distinct from the mutational directional imbalance defined above. Robustness to the threshold was assessed by repeating the analysis at ±0.2, ±0.3, ±0.5, ±0.6, and ±0.8 and with the copy-number caller's native gain/loss calls, and pair rankings were compared by Spearman correlation. Uncertainty around cohort-level medians was quantified by non-parametric bootstrap resampling of patients (10,000 resamples, percentile method), and 95% confidence intervals are reported alongside the corresponding medians.

Continuous variables are summarized as median and interquartile range and categorical variables as counts and proportions; given the sample size, formal hypothesis testing was restricted to pairwise and omnibus contrasts among cases of comparable mutational burden, and true pairs were compared with the mismatched-pair background. All analyses were conducted using Python 3.10; purity and ploidy inference used R 4.4.3. Data processing and metric computation were implemented using pandas (v2.3.3), numpy (v2.2.6) and scipy (v1.15.3), and visualizations were generated with matplotlib (v3.10.7) and the CoMut package (v0.0.3) for oncoprint-style genomic displays. Case-level descriptions in the Results are illustrative of the range of paired-tumor configurations observed and are not corrected for multiple comparisons; with 21 pairs, extreme values are expected by chance, and individual cases should not be read as formal between-group comparisons.

Code availability

Custom code used for the analyses reported in this study is available from the corresponding author upon reasonable request.

Data availability

Aggregate data supporting the findings of this study are provided in the article and its Supplementary Information. Additional de-identified data are available from the corresponding author upon reasonable request, subject to institutional approval and applicable data-sharing agreements.

Acknowledgements

This work was supported by the Italian Association for Cancer Research (AIRC) – Next Gen Clinician Scientist Grant 2024 – Ref. 31692 – P.I. Camilla Nero, and by the Italian Ministry of Health – Ricerca Corrente funds. The funders had no role in study design, data collection, analysis, interpretation of data, or writing of the manuscript.

Author contributions

A.G., L.M., C.N. and F.C. conceived the study and designed the study workflow. F.C. assembled the clinical cohort and curated the clinical annotations. A.G., M.K., and T.M. performed bioinformatic, computational, and statistical analyses. L.M. and A.D. performed the pathological assessment, including review of hematoxylin and eosin-stained slides. IM, contributed to data collection, S.D. supported clinical data collection and retrieval. M.D.B. and A.M. were responsible for genomic sequencing and molecular reporting. A.G. and F.C. co-led the study. All authors contributed to drafting and/or critically revising the manuscript and approved the final version. I. M., A.S., A.D.A., I.V., R.T., G.S., I. M., G.F.Z., F.F. and A.F. contributed to the revision of the manuscript. All authors read and approved the final manuscript.

Competing interests

C.N. declares travel support from MSD, Illumina, Menarini, AZand honoraria from Veeva, GSK, MSD, AZ, Altems, Illumina and Guardant Health.

F.F. reports research funding from Clovis, GSK, MSD and PharmaMar, personal and financial interests with GSK, MSD, SYSMEX, STRYKER ,G.S. reports research support from MSD and honoraria from Clovis Oncology, consultant for Tesaro and Johnson&Johnson.

All other authors have declared no conflicts of interest.

Bibliography

1. Berek JS, Matias-Guiu X, Creutzberg C, et al. FIGO staging of endometrial cancer: 2023. Int J Gynaecol Obstet Off Organ Int Fed Gynaecol Obstet. 2023;162(2):383-394. doi:10.1002/ijgo.14923

2. Hanna RK, Zhou C, Malloy KM, et al. Metformin potentiates the effects of paclitaxel in endometrial cancer cells through inhibition of cell proliferation and modulation of the mTOR pathway. Gynecol Oncol. 2012;125(2):458-469. doi:10.1016/j.ygyno.2012.01.009

3. Zaino R, Whitney C, Brady MF, DeGeest K, Burger RA, Buller RE. Simultaneously detected endometrial and ovarian carcinomas--a prospective clinicopathologic study of 74 cases: a gynecologic oncology group study. Gynecol Oncol. 2001;83(2):355-362. doi:10.1006/gyno.2001.6400

4. Young RH, Scully RE. Metastatic tumors in the ovary: a problem-oriented approach and review of the recent literature. Semin Diagn Pathol. 1991;8(4):250-276.

5. Ulbright TM, Roth LM. Metastatic and independent cancers of the endometrium and ovary: a clinicopathologic study of 34 cases. Hum Pathol. 1985;16(1):28-34. doi:10.1016/s0046-8177(85)80210-0

6. Schultheis AM, Ng CKY, De Filippo MR, et al. Massively Parallel Sequencing-Based Clonality Analysis of Synchronous Endometrioid Endometrial and Ovarian Carcinomas. J Natl Cancer Inst. 2016;108(6):djv427. doi:10.1093/jnci/djv427

7. Anglesio MS, Wang YK, Maassen M, et al. Synchronous Endometrial and Ovarian Carcinomas: Evidence of Clonality. J Natl Cancer Inst. 2016;108(6):djv428. doi:10.1093/jnci/djv428

8. Anglesio MS, Wang YK, Maassen M, et al. Synchronous Endometrial and Ovarian Carcinomas: Evidence of Clonality. J Natl Cancer Inst. 2016;108(6):djv428. doi:10.1093/jnci/djv428

9. Turashvili G, Gómez-Hidalgo NR, Flynn J, et al. Risk-based stratification of carcinomas concurrently involving the endometrium and ovary. Gynecol Oncol. 2019;152(1):38-45. doi:10.1016/j.ygyno.2018.10.033

10. Reijnen C, Küsters-Vandevelde HVN, Ligtenberg MJL, et al. Molecular profiling identifies synchronous endometrial and ovarian cancers as metastatic endometrial cancer with favorable clinical outcome. Int J Cancer. 2020;147(2):478-489. doi:10.1002/ijc.32907

11. Sakamoto I, Hirotsu Y, Amemiya K, Nozaki T, Mochizuki H, Omata M. Elucidation of genomic origin of synchronous endometrial and ovarian cancer (SEO) by genomic and microsatellite analysis. J Gynecol Oncol. 2023;34(1):e6. doi:10.3802/jgo.2023.34.e6

12. Reijnen C, Küsters-Vandevelde HVN, Ligtenberg MJL, et al. Molecular profiling identifies synchronous endometrial and ovarian cancers as metastatic endometrial cancer with favorable clinical outcome. Int J Cancer. 2020;147(2):478-489. doi:10.1002/ijc.32907

13. Moukarzel LA, Da Cruz Paula A, Ferrando L, et al. Clonal relationship and directionality of progression of synchronous endometrial and ovarian carcinomas in patients with DNA mismatch repair-deficiency associated syndromes. Mod Pathol Off J U S Can Acad Pathol Inc. 2021;34(5):994-1007. doi:10.1038/s41379-020-00721-6

14. Moukarzel LA, Da Cruz Paula A, Ferrando L, et al. Clonal relationship and directionality of progression of synchronous endometrial and ovarian carcinomas in patients with DNA mismatch repair-deficiency associated syndromes. Mod Pathol Off J U S Can Acad Pathol Inc. 2021;34(5):994-1007. doi:10.1038/s41379-020-00721-6

15. Southworth E, Thomson JP, Croy I, et al. Whole exome sequencing reveals diverse genomic relatedness between paired concurrent endometrial and ovarian carcinomas. Eur J Cancer. 2024;208:114205. doi:10.1016/j.ejca.2024.114205

16. Gulhan DC, Lee JJK, Melloni GEM, Cortés-Ciriano I, Park PJ. Detecting the mutational signature of homologous recombination deficiency in clinical samples. Nat Genet. 2019;51(5):912-919. doi:10.1038/s41588-019-0390-2

17. Gupta A, Gazzo A, Selenica P, et al. APOBEC3 mutagenesis drives therapy resistance in breast cancer. Nat Genet. 2025;57(6):1452-1462. doi:10.1038/s41588-025-02187-1

18. Nero C, Trozzi R, Persiani F, et al. POLE mutations in endometrial carcinoma: Clinical and genomic landscape from a large prospective single-center cohort. Cancer. 2025;131(3):e35731. doi:10.1002/cncr.35731

19. Peters EEM, Nucci MR, Gilks CB, McCluggage WG, Bosse T. Practical guidance for assessing and reporting lymphovascular space invasion (LVSI) in endometrial carcinoma. Histopathology. 2025;86(2):173-182. doi:10.1111/his.15272

20. Nero C, Salvatore L, Duranti S, et al. Concordance Analysis of Microsatellite Instability via NGS and Mismatch Repair Deficiency via IHC in Endometrial and Colorectal Cancer. Target Oncol. 2026;21(2):285-297. doi:10.1007/s11523-026-01197-1

21. Singh N. Synchronous tumours of the female genital tract. Histopathology. 2010;56(3):277-285. doi:10.1111/j.1365-2559.2009.03367.x

22. Parrillo C, Kulesko M, Persiani F, et al. Varan: a tool for managing mutational data and creating cancer studies in cBioPortal. NAR Genomics Bioinforma. 2025;7(3):lqaf107. doi:10.1093/nargab/lqaf107

23. Chakravarty D, Gao J, Phillips SM, et al. OncoKB: A Precision Oncology Knowledge Base. JCO Precis Oncol. 2017;2017:PO.17.00011. doi:10.1200/PO.17.00011

24. Selenica P, Marra A, Choudhury NJ, et al. APOBEC mutagenesis, kataegis, chromothripsis in EGFR-mutant osimertinib-resistant lung adenocarcinomas. Ann Oncol Off J Eur Soc Med Oncol. 2022;33(12):1284-1295. doi:10.1016/j.annonc.2022.09.151

25. Riester M, Singh AP, Brannon AR, et al. PureCN: copy number calling and SNV classification using targeted short read sequencing. Source Code Biol Med. 2016;11:13. doi:10.1186/s13029-016-0060-z

26. Kuzbari Z, Bandlamudi C, Loveday C, et al. Germline-focused analysis of tumour-detected variants in 49,264 cancer patients: ESMO Precision Medicine Working Group recommendations. Ann Oncol Off J Eur Soc Med Oncol. 2023;34(3):215-227. doi:10.1016/j.annonc.2022.12.003

Supplementary Files

This is a list of supplementary files associated with this preprint. Click to download.

- SupplementaryInformation1.pdf